Challenges to magnetic doping of thin films of the Dirac semimetal Cd₃As₂

Run Xiao , ¹ Jacob T. Held , ² Jeffrey Rable, ¹ Supriya Ghosh, ² Ke Wang, ³ K. Andre Mkhoyan , ² and Nitin Samarth , ¹ Department of Physics, The Pennsylvania State University, University Park, PA 16802, USA

² Department of Chemical Engineering and Materials Science, University of Minnesota, Minneapolis, MN 55455, USA

³ Materials Research Institute, The Pennsylvania State University, University Park PA 16802

(Received 20 December 2021; accepted 9 February 2022; published 22 February 2022)

Magnetic doping of topological quantum materials provides an attractive route for studying the effects of time-reversal symmetry breaking. Thus motivated, we explore the introduction of the transition metal Mn into thin films of the Dirac semimetal Cd_3As_2 during growth by molecular beam epitaxy. Scanning transmission electron microscopy measurements show the formation of a Mn-rich phase at the top surface of Mn-doped Cd_3As_2 thin films grown using both uniform doping and delta doping. This suggests that Mn acts as a surfactant during epitaxial growth of Cd_3As_2 , resulting in phase separation. Magnetometry measurements of such samples indicate a ferromagnetic phase with out-of-plane magnetic anisotropy. Electrical magneto-transport measurements of these films as a function of temperature, magnetic field, and chemical potential reveal a lower carrier density and higher electron mobility compared with pristine Cd_3As_2 films grown under similar conditions. This suggests that the surfactant effect might also serve to remove impurities from the bulk of the film. We observe robust quantum transport (Shubnikov-de Haas oscillations and an incipient integer quantum Hall effect) in very thin (7 nm) Cd_3As_2 films despite being in direct contact with a structurally disordered surface ferromagnetic overlayer.

DOI: 10.1103/PhysRevMaterials.6.024203

I. INTRODUCTION

Magnetic doping of quantum materials such as semiconductors and topological insulators (TIs) is a well-established route to the discovery of interesting emergent quantum phenomena [1–5]. Magnetically doped semiconductors such as (Ga, Mn)As have provided an important platform for proof-of-concept spintronic devices [6] while magnetic doping of certain TIs has led to the discovery of the quantum anomalous Hall effect [7–9]. In the latter case, the key physics is driven by the breaking of time-reversal symmetry by ferromagnetic order induced by the exchange interaction between transition metal dopants (Cr, V, Mn, and Fe) and the extended band states of the TI in the (Bi, Sb)₂(Te, Se)₃ family.

The success of transition metal doping of semiconductors and TIs provides a strong motivation for exploring similar magnetic doping of other topological materials such as topological Dirac semimetals [10–15]. Topological Dirac semimetals host three-dimensional (3D) Dirac fermions and can be identified as a parent phase of other topological phases, for instance, Weyl semimetals [16,17]. Introducing magnetic dopants into a Dirac semimetal to break the time-reversal symmetry could lead to the degenerate Dirac fermions separating into two (or four) Weyl fermions and a Weyl semimetal phase [18].

In the past decade, Cd_3As_2 has been theoretically predicted [19] and experimentally demonstrated [12–14] to be a Dirac semimetal. High-quality Cd_3As_2 thin films have been successfully grown using molecular beam epitaxy (MBE) [20–22] and exhibit the quantum Hall effect [21,23,24]. In a recent study, we also used *in vacuo* angle resolved photoemission

spectrscopy (ARPES) to show that MBE-grown Cd₃As₂ films (30 nm thick) exhibit a Dirac semimetal band structure identical to that seen in bulk crystals [25]. The past success of MBE growth of magnetically doped semiconductors provides a strong motivation to explore magnetic doping of MBE-grown Cd₃As₂ thin films as a route toward breaking time-reversal symmetry [18] for realizing novel topological phases such as magnetic Weyl semimetals [26–28] and monopole superconductors [29]. Prior investigations on magnetically doped Cd₃As₂ have been very limited, both in bulk crystals [30] and in thin films [31,32]. We are aware of only two published reports on attempts to magnetically dope Cd₃As₂ thin films using Cr [31] and Mn [32]. These studies principally relied on electrical magnetoresistance (MR) measurements to draw conclusions about the effect of magnetic dopants on the Dirac semimetal states and assumed that the magnetic dopants were homogeneously distributed throughout the Cd₃As₂ film.

In this paper, we describe our attempts to use MBE to dope Mn into the Dirac semimetal Cd_3As_2 . We present a systematic structural and magnetic study of heterostructures using high-angle annular dark-field scanning transmission electron microscopy (HAADF-STEM), energy dispersive x-ray spectroscopy (EDX), atomic force microscopy (AFM), high-resolution x-ray diffraction (XRD), superconducting quantum interference device (SQUID) magnetometry, and electrical transport. We find that instead of being incorporated into the Cd_3As_2 lattice, the Mn dopants form a Mn-rich layer on the top of the Cd_3As_2 layer. The Mn-rich layer shows insulating behavior and lowers the carrier density in the Cd_3As_2 layer underneath. Remarkably, even though the Mn-rich phase/ Cd_3As_2 heterostructure exhibits ferromagnetism at room temperature with out-of-plane

^{*}Corresponding author: nsamarth@psu.edu

anisotropy, the samples show pronounced quantum oscillations and an incipient integer quantum Hall effect at low temperature.

II. EXPERIMENTAL METHODS

The Mn-doped Cd₃As₂ thin films were grown by MBE in a Veeco EPI 930 chamber. We used epi-ready miscut semi-insulating GaAs (111)B substrates [1° toward (211)]. Elemental source materials were evaporated from standard effusion cells containing As (99.999995%), Ga(99.99999%), Sb(99.9999%), Cd (99.9999%), and Mn (99.9998%). The epiready GaAs substrates were first annealed inside the MBE chamber to flash off the native oxide at a thermocouple temperature of 720 °C (the actual temperature is likely 580 °C). Then, we deposited a thin (\sim 2 nm) GaAs layer at the same substrate temperature to smooth the surface. Subsequently, the substrates were cooled down to 480°C under As₄ flux for the growth of the GaSb buffer layer with an Sb/Ga beam equivalent pressure (BEP) ratio of 7. We note that both the GaAs and the GaSb layers are highly insulating, as confirmed by control measurements. The substrates were then cooled down to 400 °C under Sb₄ flux and further cooled down to 180 °C after closing the Sb shutter for the growth of Mn-doped Cd₃As₂. Once the sample temperature was stable at 180 °C, we used the Cd, As, and Mn effusion cells with BEP of Cd around 6×10^{-8} Torr, As around 2×10^{-8} Torr, and Mn around 1.2×10^{-9} Torr.

For cross-sectional HAADF-STEM imaging and STEM-EDX elemental mapping, we prepared TEM lamella for STEM analysis on a FEI Helios Nanolab G4 dual-beam focused ion beam (FIB). Amorphous carbon was first deposited on the films to protect the surface from damage due to exposure to the ion beam. STEM imaging and EDX spectroscopy were performed on an aberration-corrected FEI Titan G2 60-300 (S)TEM microscope equipped with a CEOS DCOR probe corrector and a super-X EDX spectrometer. The microscope was operated at 300 keV. We acquired HAADF-STEM images with a probe convergence semiangle of 25.5 mrad and detector inner and outer collection angles of 55 and 200 mrad, respectively.

Measurements of the magnetization of the thin films were carried out over a temperature range $10~{\rm K} \leqslant T \leqslant 300~{\rm K}$ and magnetic field up to $B=3~{\rm T}$ in a Quantum Design SQUID magnetometer with the sample mounted in a straw for field parallel to and field normal to the sample plane. The diamagnetic background signal of the GaAs substrate was measured separately so that its field dependence could be reliably subtracted.

For electrical transport measurements, we patterned the thin-film samples into 40 $\mu m \times 10 \, \mu m$ Hall bar devices using photolithography and Ar^+ plasma dry etching. The top gate was defined by a 30 nm Al_2O_3 dielectric layer and Ti(5 nm)/Au(50 nm) contacts deposited by atomic layer deposition and electron beam evaporation, respectively. MR and Hall effect measurements were carried out in a Quantum Design Physical Properties Measurement System over a temperature range 2 K \leqslant T \leqslant 300 K and in magnetic fields up to $B=9\,\mathrm{T}$.

III. RESULTS AND DISCUSSION

We attempted to grow Mn-doped Cd₃As₂ thin films using two methods: Uniform doping wherein the Mn flux is constant during the growth of Cd₃As₂ and the delta doping method wherein we interrupt the growth of Cd₃As₂ and deposit a fractional monolayer of MnAs. The latter approach has been effective in magnetic doping of II-VI and III-V semiconductors [33,34]. While we focus our discussion of structural characterization on a sample grown using the uniform doping method, we note that both growth methods resulted in films with similar characteristics. Reflection high-energy electron diffraction (RHEED) measurements during the growth showed streaky patterns in either approach, indicating a relatively flat surface with some disorder even when depositing a Mn-rich layer [Fig. 1(a)]. Postgrowth, we carried out ex situ AFM measurements [Fig. 1(b)] that indicated a rootmean-square surface roughness of 1.77 nm over an area of $10 \times 10 \,\mu\text{m}^2$. The steps in the AFM image are due to the miscut substrate; these help prevent twinning defects and improve the quality of the sample. The $1 \times 1 \mu m^2$ AFM image in Fig. 1(b) shows the atomic steps of the heterostructure, indicative of the epitaxial growth of the heterostructure. Figure 1(c) compares the XRD scan of a nominally uniformly Mn-doped Cd₃As₂ film of nominal 25 nm thickness; the plot compares this XRD scan with that of a pristine Cd₃As₂ film. We observe extra diffraction peaks in the Mn-doped film suggesting the presence of an extra phase. However, from the XRD scan alone, we are unable to identify the crystal structure of this phase.

To understand the crystalline structure and elemental distribution within the heterostructures, we now discuss the TEM measurements obtained from a uniformly Mn-doped Cd₃As₂ film of nominal 15 nm thickness. Measurements taken on a delta-doped film of similar thickness yield qualitatively similar results (see Fig. S1 in the Supplemental Material [35]).

High magnification HAADF-STEM images of the film cross-section revealed a crystalline Mn-Cd₃As₂ film of thickness \sim 13 nm, epitaxial to the GaSb substrate [Fig. 2(a)]. A uniform amorphous-like layer (\sim 5 nm thick) of darker contrast is seen on top of the film. STEM-EDX elemental mapping, shown in Fig. 2(a), was used to obtain compositional information from the heterostructure. Surprisingly, instead of incorporating Mn throughout the film, the growth procedure, illustrated in Fig. 2(b), produced a segregated Mn-rich phase at the top surface of the Cd₃As₂ film. The resultant structure is visible in the EDX maps and illustrated in Fig. 2(c).

Averaging the results from several STEM-EDX data sets revealed that the darker contrast region seen in STEM images on top of the Cd₃As₂ film is primarily composed of a Mn-oxide phase with small traces of Cd and As (O: 49 at%, Mn: 39 at%; Cd and As: 12 at%). While most of the Mn migrated to the surface, EDX analysis revealed <5 at% Mn content in the Cd₃As₂ film layer, indicating some doping of the films with Mn. In addition to the uniform Mn-rich layer, some regions exhibited islands rising out of the film surface with more mixing between Mn, Cd, and As (Cd: 17.3 at%, Mn: 27.4 at%, O: 24.5 at%, As: 29.8 at%). These islands were mostly amorphous with some crystalline regions closer to the surface of the film. The phase separation seen from

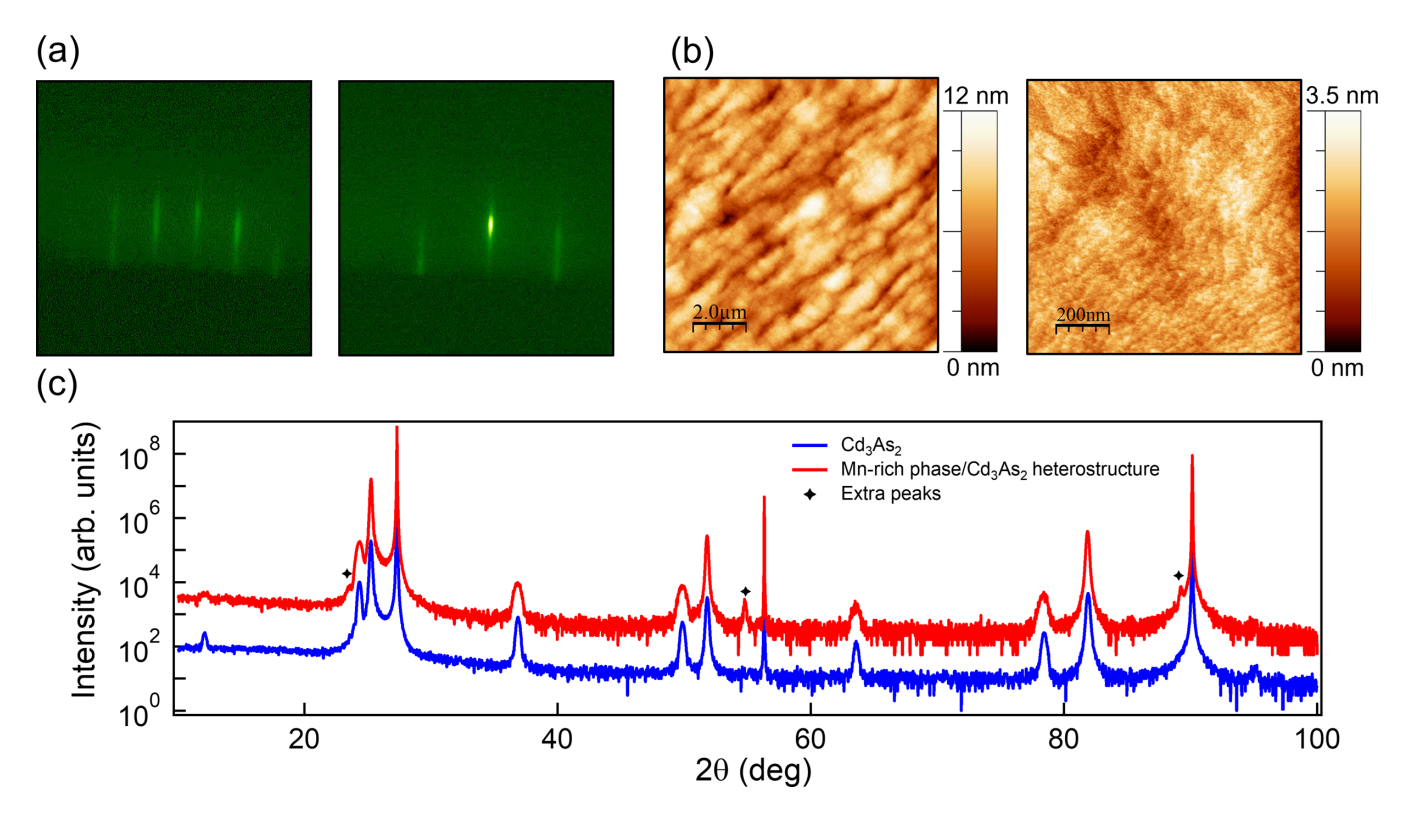


FIG. 1. (a) In situ RHEED patterns during MBE of a nominally 15-nm-thick Mn-doped Cd_3As_2 heterostructure grown using the uniform doping approach. The electron beam is directed along $[0\overline{1}1]$ (left) and $[\overline{2}11]$ (right) direction. (b) Ex situ AFM images of the same sample as in panel (a). (c) Out-of-plane XRD of a nominally 25-nm-thick Mn-doped Cd_3As_2 heterostructure grown using the uniform Mn-doping approach. The "extra peaks" in the XRD indicate the presence of a Mn-rich phase of unknown composition.

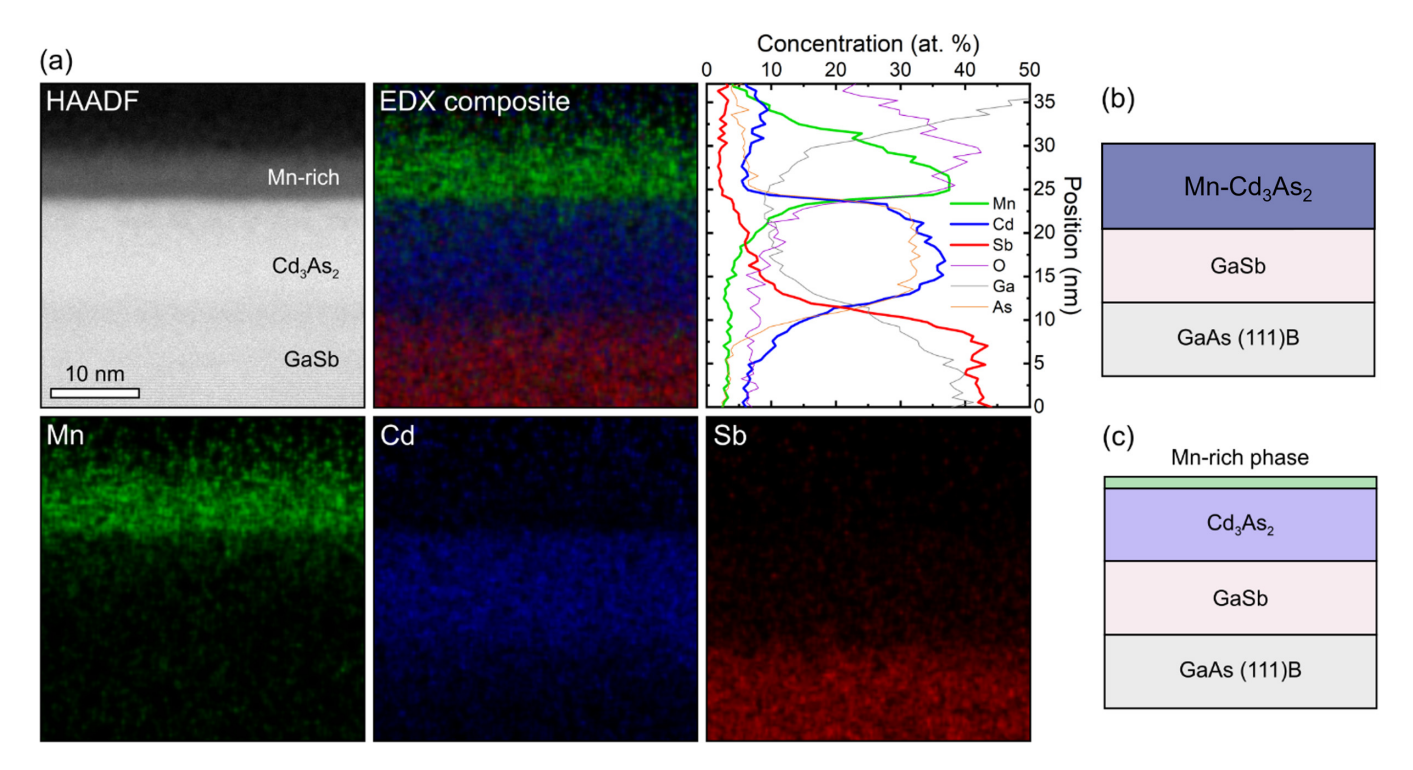


FIG. 2. (a) Low-magnification cross-sectional HAADF-STEM image of a Mn-rich phase/ Cd_3As_2 heterostructure that results from uniform Mn-doping during MBE growth of Cd_3As_2 . Composite and individual EDX maps show the spatial distribution of Mn, Cd, and Sb in the heterostructure as well as an atomic percent concentration profile across the heterostructure. Instead of being incorporated into the Cd_3As_2 lattice, a segregated Mn-rich phase formed on the top of the Cd_3As_2 layer. (b) Schematic of the intended sample using the uniform doping method. (c) Schematic of the actual Mn-rich phase/ Cd_3As_2 heterostructure produced by the uniform doping growth.

the STEM-EDX data is supported by the low solubility of Mn in Cd₃As₂. As a result, even for the MBE growth under nonequilibrium conditions, it is hard to overcome the kinetic barrier to form Mn-doped Cd₃As₂ [36].

Since our attempt to introduce magnetic dopants into Cd₃As₂ thin films inadvertently resulted in a phase-segregated heterostructure wherein a Mn-rich compound is cleanly interfaced with a Cd₃As₂ film, two important questions arise. First, is the Mn-rich phase magnetically ordered? If so, how does its presence affect the electronic transport properties of the Cd₃As₂ film with which it is directly interfaced? Naively, one might anticipate that interfacial exchange interaction between the magnetic moments in the overlayer and the band electrons in the Cd₃As₂ film would result in a degradation of the mobility due to spin-dependent scattering. We now address the magnetic and electrical transport properties of these Mn-doped Cd₃As₂ films. Since we have established that the actual sample structure consists of a thin Mn-rich overlayer interfaced with a Cd₃As₂ film regardless of the growth method used, we will refer to the samples being measured as heterostructures with x nm Mn-rich layer/y nm Cd₃As₂.

We first discuss SQUID magnetometry measurements of a 1 nm Mn-rich layer/7 nm Cd₃As₂ heterostructure that results from the delta-doping method with 6 repeats of (submonolayer MnAs/1.25 nm Cd₃As₂); the thicknesses in the final structure are estimated from HAADF-STEM measurements of a thicker sample using similar conditions with twice the thickness. Figure 3(a) shows the magnetization (M) versus field (H) at $T = 10 \,\mathrm{K}$ for this sample with the field in plane and out of plane. A diamagnetic background has been subtracted in these plots. Zoomed-in views of M versus H for field in plane [Fig. 3(b)] and out of plane [Fig. 3(c)] show hysteresis loops with a very large coercive field (~80 mT) in the former case and a much smaller coercive field (~10 mT) in the latter. The behavior of the coercive field and the saturation field for the two field orientations are consistent with ferromagnetism in the sample with a strong out-of-plane magnetocrystalline anisotropy. This could arise from an inhomogeneous distribution of Mn forming complex nanoscale cluster phases with the other elements present in the TEM analysis (primarily O, but also containing Cd and As). We note that the most commonly known compounds involving Mn and O (MnO and Mn₃O₄) are antiferromagnetic and ferromagnetic, respectively. A more detailed understanding of the origin of ferromagnetism in such samples will require measurements such as x-ray magnetic circular dichroism and polarized neutron reflectometry.

Next, we discuss electrical transport in this 1 nm Mn-rich layer/7 nm Cd_3As_2 heterostructure. All the MR and Hall effect data shown have been properly field symmetrized or antisymmetrized, respectively. Figure 3(d) shows the results of such measurements at T=2 K. Surprisingly, despite the presence of the ferromagnetic overlayer in direct contact with the Cd_3As_2 film, we observe pronounced quantum oscillations and even an incipient quantum Hall effect indicated by a Hall resistance plateau corresponding to $\rho_{xy} = \frac{1}{6} \frac{h}{e^2} = 4.3 \text{ k}\Omega$. The latter indicates that the quantum transport is produced by a 2D electron gas, a conclusion further confirmed via MR measurements at different orientations of the magnetic field from the sample normal (see Fig. S2 in the Supplemental Material

[35]). We searched for possible signatures of an exchange coupling between the electrons in the Cd₃As₂ layer and Mn moments in the overlayer. Since the easy axis of the Mn-rich layer is out-of-plane according to our SQUID measurements, an exchange coupling between carriers in Cd₃As₂ and the Mn moments should lead to hysteresis in the field dependence of the Hall resistance and also to the MR from modifications to the quantum corrections to diffusive transport. Figure 3(e) shows a careful sweep of the longitudinal MR and the Hall effect in the field range $-0.1 \text{ T} \leq B \leq 0.1 \text{ T}$. The low-field MR shows a nonmonotonic dependence on magnetic field with an initial positive MR followed by a sudden change to a negative MR at a field close to the coercive field observed in SQUID magnetometry. The negative MR at fields higher than the saturation field of the ferromagnetic layer may indicate a reduction in spin-dependent scattering. In contrast, pristine Cd₃As₂ films grown under similar conditions only show a positive MR for field perpendicular to the sample plane (see Fig. S3 in the Supplemental Material). We do not see any obvious signs of hysteretic or nonlinear Hall resistance. It is possible that with the step size used in the magnetotransport measurements (0.01 T), we might not be able to resolve these differences given how quickly the magnetization saturates with field along the anisotropy axis and the narrowness of hysteresis loop.

To further understand the effect of the Mn-rich overlayer on quantum transport, we analyzed the quantum oscillations in the heterostructure and compared the behavior with MR measurements in pure Cd₃As₂ thin films grown under similar conditions. For the 1 nm Mn-rich layer/7 nm Cd₃As₂ heterostructure, the amplitude of quantum oscillations gradually decreased with increasing temperature but remained finite up to about $T = 100 \,\mathrm{K}$ as shown in Fig. 4(a). We note that the v = 6 quantum Hall plateau mentioned earlier was observable up to $T = 20 \,\mathrm{K}$ in Fig. 4(b). To extract the carrier density, mobility, and effective mass of the carriers involved in quantum transport, we studied the temperature dependence of the quantum oscillations [Figs. 4(c) and 4(d)]. The carrier density and mobility were calculated using both the Drude model and the quantum oscillations. Using the Drude model, we find a carrier density $n = 9.5 \times 10^{11} \text{cm}^{-2}$ and a mobility $\mu = 9200 \text{ cm}^2/\text{Vs}$ at T = 2 K. The analysis of quantum oscillations yields $n = 7.2 \times 10^{11} \text{cm}^{-2}$. The higher carrier density deduced from Drude analysis compared with that obtained from quantum oscillations indicates the presence of low mobility carriers that do not contribute to the quantum oscillations. The band origin of the low mobility carriers is not clear at this stage. By fitting magnetic field and temperature dependence of the amplitude of the quantum oscillations using the standard Lifshitz-Kosevich formula [21], we extracted an effective mass $m^* = 0.04m_e$ and a quantum mobility $\mu_q =$ 1016 cm²/Vs. This light effective mass is due to the Dirac dispersion and is in good agreement with previous studies of Cd_3As_2 thin films [21,23,37].

Figure 4(c) also shows the carrier density and the mobility of a pure 7 nm Cd_3As_2 thin film (at T = 2K) calculated from the Drude model; this film was grown under nominally identical conditions (substrate temperature and Cd:As flux ratio) to those used for the growth of Mn-delta-doped samples. The carrier density in the pure film is about 20% higher and the

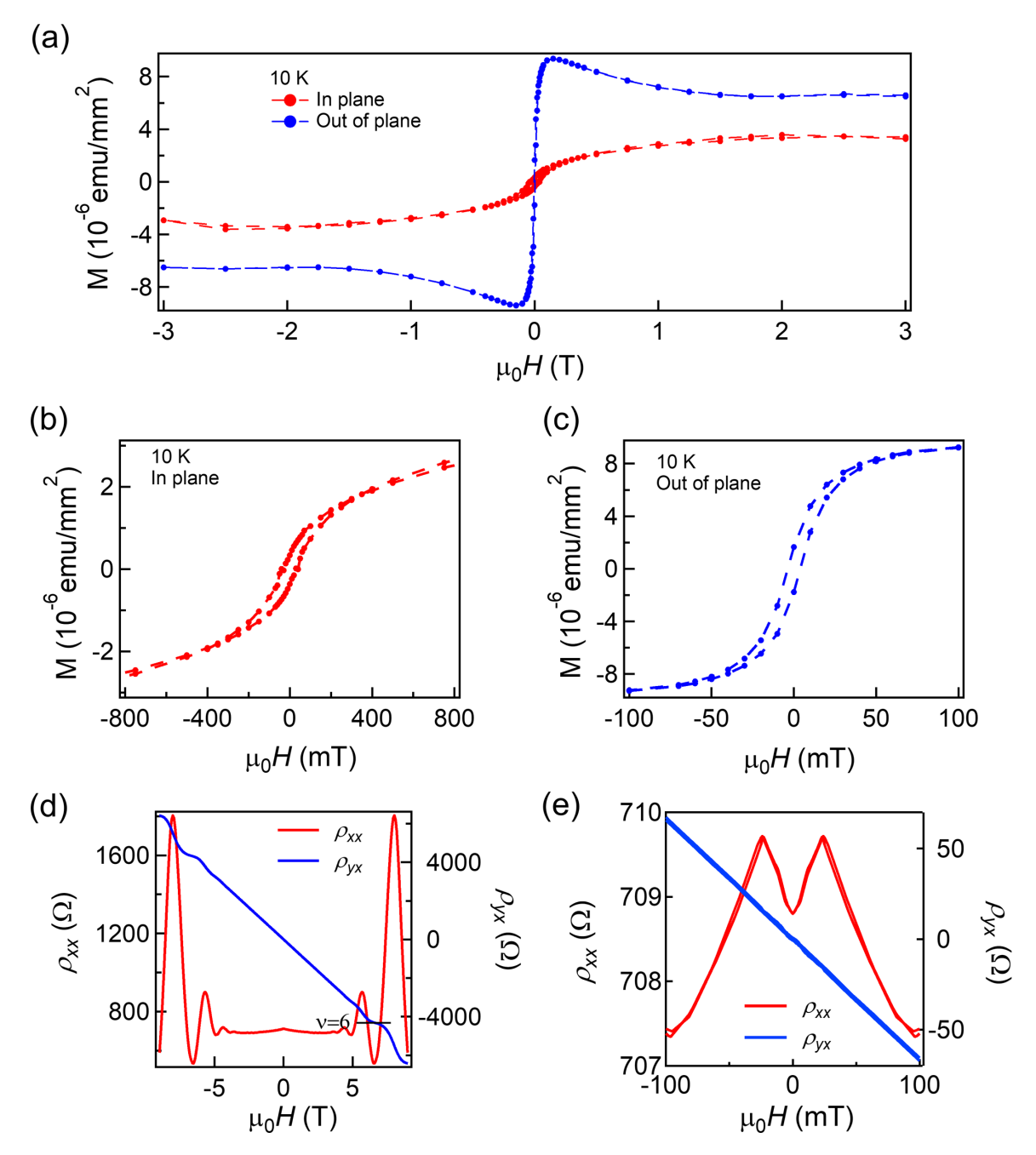


FIG. 3. Investigation of ferromagnetism in a Mn-rich layer/ Cd_3As_2 heterostructure. (a)–(c) SQUID magnetometry measurements of a 1 nm Mn-rich phase/7 nm Cd_3As_2 heterostructure at 10 K, respectively. The data suggest ferromagnetic ordering with an out-of-plane magnetic anisotropy. The inconsistency between the saturated magnetization values in the easy- and hard-axis measurements is an artifact created by the difficulty in properly handling the large filling factor when the thin film is mounted for field in plane measurements in the SQUID. (d) Observation of Shubnikov de Haas oscillations and an incipient integer quantum Hall effect in a 1 nm Mn-rich phase/7 nm Cd_3As_2 heterostructure at 2 K. (e) An expanded view of the low-field MR and Hall effect in panel (d).

Drude mobility is about 50% lower than in the Mn-doped film. This combination of lower mobility and higher carrier density leads to an absence of quantum oscillations at the magnetic fields used on our study (see data in Fig. S3 of the Supplemental Material [35]). Our findings suggest that the Mn-rich layer does not contribute to the transport signal and perhaps passivates the Cd₃As₂ layers underneath from electronegative OH-surface adsorbates [38]. We also speculate that the presence of Mn dopants during growth may

limit the arsenic deficiency which is believed to contribute to electron doping, thus leading to a lower carrier density.

Although the Mn-rich layer lies between the Cd_3As_2 layer and the top gate, it does not appear to affect the efficiency of an electrostatic top gate. As shown in Figs. 4(e) and 4(f), the chemical potential of the heterostructure can be tuned from n-type to p-type by applying a top gate voltage to move the chemical potential through the charge neutral point. Based on our past ARPES measurements in pristine Cd_3As_2 thin films

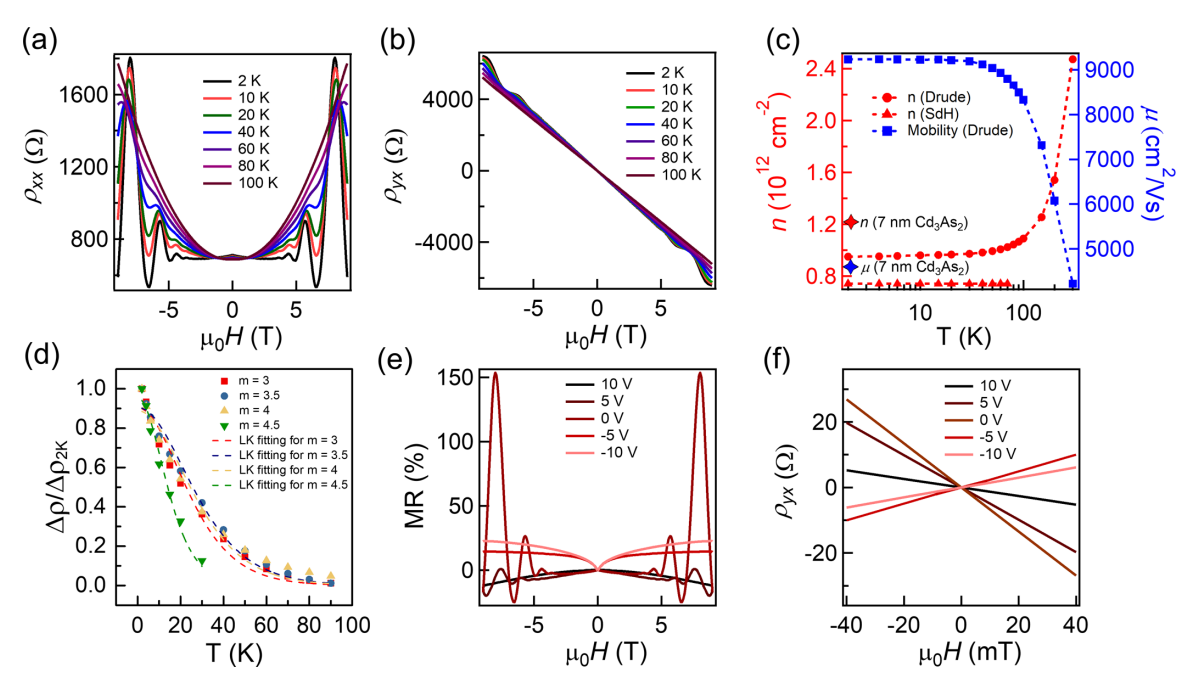


FIG. 4. Shubnikov-de Haas quantum oscillations in a 1 nm Mn-rich phase/7 nm Cd_3As_2 heterostructure. (a), (b) The temperature dependence of the quantum oscillations and Hall effect, respectively. (c) Temperature dependence of the carrier density and Drude mobility. The values of the carrier density and Drude mobility for a pristine Cd_3As_2 film of the same thickness are also shown at 2 K for comparison. (d) Temperature dependence of the quantum oscillation amplitude at different Landau fan index (m = 3, 3.5, 4, 4.5), with integer and half-integer values of m corresponding to MR peaks and valleys, respectively. Figure S4 in the Supplemental Material [35] shows the oscillations in more detail. The dashed lines are fits using the well-known Lifshitz-Kosevich formula. (e), (f) Gate-voltage dependence of the quantum oscillations and Hall effect, respectively.

[25], it is reasonable to identify this charge neutral point as the Dirac node or, more likely, its vestige in the quantum confined thin-film regime. We only observed quantum oscillations in the positive gate voltage regime and not at negative gate voltage. This is consistent with quantum transport being dominated by high mobility *n*-type carriers when the chemical potential is positioned above the charge neutral point as opposed to contributions from low mobility *p*-type carriers when the chemical potential lies below the charge neutral point. We also note that the incipient quantum Hall plateau is only observable only around the charge neutral point near zero gate voltage.

We now discuss our quantum transport results in the context of prior experimental studies of quantum oscillations and the quantum Hall effect in pristine (nonmagnetic) Cd₃As₂ thin films. The observation of the integer quantum Hall effect in various Cd₃As₂ thin films of varying thickness (10–70 nm) and on different substrates [21,23,39] clearly indicates quantum transport occurs in a 2D electron system. However, a complete understanding of its origin in the different experimentally studied regimes of film thickness is still lacking. In Cd₃As₂ films of sufficient thickness to still preserve the Dirac point, quantum oscillations and the quantum Hall effect can arise from Weyl orbits that connect doubled surface Fermi arcs on the top and bottom surfaces [40]. A recent systematic study of the thickness-dependence of the quantum transport in top-gated Cd₃As₂ thin films in the thickness range 10-60 nm cautions against the ready interpretation of experimental observations in terms of Weyl orbits [24]. The quantum Hall effect in Cd₃As₂ thin films can also arise from 2D quantum confined bulk states [19], topological surface states (closed surface Fermi pockets) [41], or surface Fermi arcs [42]. The density functional theory calculations reported in the last reference indicate that surface Fermi arcs likely survive in Cd₃As₂ films down to the thicknesses studied experimentally here [42]. At this stage, we do not have sufficient data to rigorously distinguish between these various scenarios. But could the survival of clear quantum transport in the presence of a highly structurally disordered ferromagnetic interface at the top surface provide some insights? Any 2D states on the top surface, whether topological or trivial in nature, would presumably be significantly perturbed in the presence of the disordered magnetic layer. For example, the out-of-plane magnetization in the Mn-rich top layer would break time-reversal symmetry if exchange-coupled with the top surface states in Cd₃As₂ while spin-dependent scattering would presumably lower the mobility of both trivial and topological states. It is worthwhile pointing out that the quantum Hall effect behavior in our Mn-Cd₃As₂ heterostructures has similar characteristics to that observed in pristine Cd₃As₂ films of slightly greater thickness (10-12 nm) measured by others [21,23,39]: for instance, we only observe quantum oscillations corresponding to even filling factors under similar temperature and magnetic field regimes. Our results suggest that the wave function of the 2D electron system contributing to the quantum Hall effect in ultrathin Cd₃As₂ films has a maximum located away from the top and bottom surfaces, thus being immune to perturbation by the magnetism on the top surface. At this stage, however, we do not have a rigorous calculation to support this speculation in detail.

IV. SUMMARY

In summary, we have shown that a conventional magnetic doping approach to introducing ferromagnetism into Cd₃As₂ by MBE results in a phase separation with a Mn-rich nearsurface layer capping a pristine Cd₃As₂ film since Mn likely acts as surfactant. The Mn-rich region shows out-of-plane magnetic anisotropy in SQUID measurements. Surprisingly, this ferromagnetic Mn-rich layer does not adversely affect the quantum transport in the Cd₃As₂ underneath. On the contrary, compared with pure Cd₃As₂ thin films grown under identical conditions, the presence of the Mn surfactant lowers the carrier density so that the chemical potential is close to the charge neutral point and leads to an enhanced electron mobility. The resulting 1 nm Mn-rich layer/7 nm Cd₃As₂ films show an incipient quantum Hall effect in transport measurements. This should become more robust if the samples are measured at lower temperature and at higher magnetic fields. Measurements at dilution fridge temperatures may also reveal emergent physics resulting from the presence of the ferromagnetic overlayer. Although it is hard to dope Mn directly into Cd₃As₂ using MBE, it is worthwhile to use other techniques such as polarized-neutron reflectometry to search for magnetic proximity effects of the ferromagnetic top layer on the Cd₃As₂ underneath. Our study indicates that extreme caution is called for in relying on magnetotransport data alone as a sign of broken time-reversal symmetry in magnetically doped Cd₃As₂ films, especially in the absence of electron microscopy data [31].

ACKNOWLEDGMENTS

This work was principally supported as part of the Institute for Quantum Matter, an Energy Frontier Research Center funded by the U.S. Department of Energy, Office of Science, Basic Energy Sciences under Award No. DE-SC0019331 (R.X., N.S.) The magnetometry measurements were supported by a grant from the University of Chicago (J.R., N.S.). The electron microscopy effort (J.H., A.M.) was supported by SMART, one of seven centers of nCORE, a Semiconductor Research Corporation program, sponsored by the National Institute of Standards and Technology (NIST) and by the College of Science and Engineering Characterization Facility, University of Minnesota, which receives partial support from the NSF through the MRSEC (Award No. DMR-2011401) and the NNCI (Award No. ECCS-2025124) programs.

- [1] A. H. Macdonald, P. Schiffer, and N. Samarth, Ferromagnetic semiconductors: Moving beyond (Ga,Mn)As, Nat. Mater. 4, 195 (2005).
- [2] C.-X. Liu, X.-L. Qi, X. Dai, Z. Fang, and S.-C. Zhang, Quantum Anomalous Hall Effect In Hg_{1-y} Mn_yTe Quantum Wells, Phys. Rev. Lett. **101**, 146802 (2008).
- [3] R. Yu, W. Zhang, H.-J. Zhang, S.-C. Zhang, X. Dai, and Z. Fang, Quantized anomalous Hall effect in magnetic topological insulators, Science 329, 61 (2010).
- [4] S.-Y. Xu, M. Neupane, C. Liu, D. Zhang, A. Richardella, L. A. Wray, N. Alidoust, M. Leandersson, T. Balasubramanian, J. Sánchez-Barriga, O. Rader, G. Landolt, B. Slomski, J. H. Dil, J. Osterwalder, T.-R. Chang, H.-T. Jeng, H. Lin, A. Bansil, N. Samarth, and M. Z. Hasan, Hedgehog spin texture and Berry's phase tuning in a magnetic topological insulator, Nat. Phys. 8, 616 (2012).
- [5] C.-Z. Chang, J. Zhang, M. Liu, Z. Zhang, X. Feng, K. Li, L.-L. Wang, X. Chen, X. Dai, Z. Fang, X.-L. Qi, S.-C. Zhang, Y. Wang, K. He, X.-C. Ma, and Q.-K. Xue, Thin films of magnetically doped topological insulator with carrier-independent long-range ferromagnetic order, Adv. Mater. 25, 1065 (2013).
- [6] T. Dietl and H. Ohno, Dilute ferromagnetic semiconductors: physics and spintronic structures, Rev. Mod. Phys. 86, 187 (2014).
- [7] C.-Z. Chang, J. Zhang, X. Feng, J. Shen, Z. Zhang, M. Guo, K. Li, Y. Ou, P. Wei, L.-L. Wang, Z.-Q. Ji, Y. Feng, S. Ji, X. Chen, J. Jia, X. Dai, Z. Fang, S.-C. Zhang, K. He, Y. Wang, L. Lu, X.-C. Ma, and Q.-K. Xue, Experimental observation of the quantum anomalous Hall effect in a magnetic topological insulator, Science 340, 167 (2013).
- [8] A. Kandala, A. Richardella, S. Kempinger, C.-X. Liu, and N. Samarth, Giant anisotropic magnetoresistance in a quantum anomalous Hall insulator, Nat. Commun. 6, 7434 (2015).

- [9] C.-Z. Chang, W. Zhao, D. Y. Kim, H. Zhang, B. A. Assaf, D. Heiman, S.-C. Zhang, C.-x. Liu, M. H. W. Chan, and J. S. Moodera, High-precision realization of robust quantum anomalous Hall state in a hard ferromagnetic topological insulator, Nat. Mater. 14, 473 (2015).
- [10] Z. K. Liu, B. Zhou, Y. Zhang, Z. J. Wang, H. M. Weng, D. Prabhakaran, S.-K. Mo, Z. X. Shen, Z. Fang, X. Dai, Z. Hussain, and Y. L. Chen, Discovery of a three-dimensional topological Dirac semimetal, Na₃Bi, Science 343, 864 (2014).
- [11] S.-Y. Xu, C. Liu, S. K. Kushwaha, R. Sankar, J. W. Krizan, I. Belopolski, M. Neupane, G. Bian, N. Alidoust, T.-R. Chang, H.-T. Jeng, C.-Y. Huang, W.-F. Tsai, H. Lin, P. P. Shibayev, F.-C. Chou, R. J. Cava, and M. Z. Hasan, Observation of Fermi arc surface states in a topological metal, Science 347, 294 (2015).
- [12] Z. K. Liu, J. Jiang, B. Zhou, Z. J. Wang, Y. Zhang, H. Weng, D. Prabhakaran, S. K. Mo, H. Peng, P. Dudin, T. Kim, M. Hoesch, Z. Fang, X. Dai, Z. X. Shen, D. L. Feng, H. Z., and Y. L. Chen, A stable three-dimensional topological Dirac semimetal Cd₃As₂, Nat. Mater. 13, 677 (2014).
- [13] M. Neupane, S.-Y. Xu, R. Sankar, N. Alidoust, G. Bian, C. Liu, I. Belopolski, T.-R. Chang, H.-T. Jeng, H. Lin, A. Bansil, F. Chou, and M. Z. Hasan, Observation of a three-dimensional topological Dirac semimetal phase in high-mobility Cd₃As₂, Nat. Commun. 5, 3786 (2014).
- [14] H. Yi, Z. Wang, C. Chen, Y. Shi, Y. Feng, A. Liang, Z. Xie, S. He, J. He, Y. Peng, X. Liu, Y. Liu, L. Zhao, G. Liu, X. Dong, J. Zhang, M. Nakatake, M. Arita, K. Shimada, H. Namatame, M. Taniguchi, Z. Xu, C. Chen, X. Dai, Z. Fang, and X. J. Zhou, Evidence of topological surface state in three-dimensional Dirac semimetal Cd₃As₂, Sci. Rep. 4, 6106 (2014).
- [15] N. P. Armitage, E. J. Mele, and A. Vishwanath, Weyl and Dirac semimetals in three-dimensional solids, Rev. Mod. Phys. 90, 015001 (2018).

- [16] H. Weyl, Elektron und gravitation. i, Z. Phys. **56**, 330 (1929).
- [17] A. A. Burkov and L. Balents, Weyl Semimetal in a Topological Insulator Multilayer, Phys. Rev. Lett. **107**, 127205 (2011).
- [18] S. Baidya and D. Vanderbilt, First-principles theory of the dirac semimetal Cd₃As₂ under Zeeman magnetic field, Phys. Rev. B **102**, 165115 (2020).
- [19] Z. Wang, H. Weng, Q. Wu, X. Dai, and Z. Fang, Three-dimensional Dirac semimetal and quantum transport in Cd₃As₂, Phys. Rev. B 88, 125427 (2013).
- [20] T. Schumann, M. Goyal, H. Kim, and S. Stemmer, Molecular beam epitaxy of Cd₃As₂ on a III-V substrate, APL Mater. **4**, 126110 (2016).
- [21] M. Uchida, Y. Nakazawa, S. Nishihaya, K. Akiba, M. Kriener, Y. Kozuka, A. Miyake, Y. Taguchi, M. Tokunaga, N. Nagaosa, Y. Tokura, and M. Kawasaki, Quantum Hall states observed in thin films of Dirac semimetal Cd₃As₂, Nat. Commun. 8, 2274 (2017).
- [22] Y. Liu, C. Zhang, X. Yuan, T. Lei, C. Wang, D. Di Sante, A. Narayan, L. He, S. Picozzi, S. Sanvito, R. Che, and F. Xiu, Gatetunable quantum oscillations in ambipolar Cd₃As₂ thin films, NPG Asia Mater. 7, e221 (2015).
- [23] T. Schumann, L. Galletti, D. A. Kealhofer, H. Kim, M. Goyal, and S. Stemmer, Observation of the Quantum Hall Effect in Confined Films of the Three-Dimensional Dirac Semimetal Cd₃As₂, Phys. Rev. Lett. 120, 016801 (2018).
- [24] L. Galletti, T. Schumann, D. A. Kealhofer, M. Goyal, and S. Stemmer, Absence of signatures of Weyl orbits in the thickness dependence of quantum transport in cadmium arsenide, Phys. Rev. B **99**, 201401(R) (2019).
- [25] W. Yanez, Y. Ou, R. Xiao, J. Koo, J. T. Held, S. Ghosh, J. Rable, T. Pillsbury, E. G. Delgado, K. Yang, J. Chamorro, A. J. Grutter, P. Quarterman, A. Richardella, A. Sengupta, T. McQueen, J. A. Borchers, K. A. Mkhoyan, B. Yan, and N. Samarth, Spin and Charge Interconversion in Dirac-Semimetal Thin Films, Phys. Rev. Appl. 16, 054031 (2021).
- [26] D. F. Liu, A. J. Liang, E. K. Liu, Q. N. Xu, Y. W. Li, C. Chen, D. Pei, W. J. Shi, S. K. Mo, P. Dudin, T. Kim, C. Cacho, G. Li, Y. Sun, L. X. Yang, Z. K. Liu, S. S. P. Parkin, C. Felser, and Y. L. Chen, Magnetic Weyl semimetal phase in a Kagomé crystal, Science 365, 1282 (2019).
- [27] N. Morali, R. Batabyal, P. K. Nag, E. Liu, Q. Xu, Y. Sun, B. Yan, C. Felser, N. Avraham, and H. Beidenkopf, Fermi-arc diversity on surface terminations of the magnetic Weyl semimetal Co₃Sn₂S₂, Science **365**, 1286 (2019).
- [28] I. Belopolski, K. Manna, D. S. Sanchez, G. Chang, B. Ernst, J. Yin, S. S. Zhang, T. Cochran, N. Shumiya, H. Zheng, B. Singh, G. Bian, D. Multer, M. Litskevich, X. Zhou, S.-M. Huang, B. Wang, T.-R. Chang, S.-Y. Xu, A. Bansil *et al.*, Discovery of

- topological Weyl fermion lines and drumhead surface states in a room temperature magnet, Science **365**, 1278 (2019).
- [29] Y. Li and F. D. M. Haldane, Topological Nodal Cooper Pairing in Doped Weyl Metals, Phys. Rev. Lett. 120, 067003 (2018).
- [30] Y. V. Goryunov and A. Nateprov, Influence of europium doping on magnetic properties of 3D topological semimetal Cd₃As₂ from ESR data, Phys. Solid State **60**, 68 (2018).
- [31] Y. Liu, R. Tiwari, A. Narayan, Z. Jin, X. Yuan, C. Zhang, F. Chen, L. Li, Z. Xia, S. Sanvito, P. Zhou, and F. Xiu, Cr doping induced negative transverse magnetoresistance in Cd₃As₂ thin films, Phys. Rev. B 97, 085303 (2018).
- [32] H. Wang, J. Ma, Q. Wei, and J. Zhao, Mn doping effects on the gate-tunable transport properties of Cd₃As₂ films epitaxied on GaAs, J. Semicond. **41**, 072903 (2020).
- [33] S. A. Crooker, D. A. Tulchinsky, J. Levy, D. D. Awschalom, R. Garcia, and N. Samarth, Enhanced Spin Interactions in Digital Magnetic Heterostructures, Phys. Rev. Lett. 75, 505 (1995).
- [34] R. K. Kawakami, E. Johnston-Halperin, L. F. Chen, M. Hanson, N. Guébels, J. S. Speck, A. C. Gossard, and D. D. Awschalom, (Ga,Mn)As as a digital ferromagnetic heterostructure, Appl. Phys. Lett. 77, 2379 (2000).
- [35] See Supplemental Material at http://link.aps.org/supplemental/ 10.1103/PhysRevMaterials.6.024203 for additional TEM and transport data.
- [36] A. I. Ril, I. V. Fedorchenko, S. F. Marenkin, A. V. Kochura, and A. E. Kuz'ko, Phase equilibria in the CdAs₂-Cd₃As₂-MnAs ternary system, Russ. J. Inorg. Chem. **62**, 976 (2017).
- [37] Y. Zhao, H. Liu, C. Zhang, H. Wang, J. Wang, Z. Lin, Y. Xing, H. Lu, J. Liu, Y. Wang, S. M. Brombosz, Z. Xiao, S. Jia, X. C. Xie, and J. Wang, Anisotropic Fermi surface and Quantum Limit Transport in High Mobility Three-Dimensional Dirac Semimetal Cd₃As₂, Phys. Rev. X 5, 031037 (2015).
- [38] L. Galletti, T. Schumann, T. E. Mates, and S. Stemmer, Nitrogen surface passivation of the Dirac semimetal Cd₃As₂, Phys. Rev. Materials **2**, 124202 (2018).
- [39] M. Goyal, L. Galletti, S. Salmani-Rezaie, T. Schumann, D. A. Kealhofer, and S. Stemmer, Thickness dependence of the quantum hall effect in films of the three-dimensional dirac semimetal Cd₃As₂, APL Mater. 6, 026105 (2018).
- [40] A. C. Potter, I. Kimchi, and A. Vishwanath, Quantum oscillations from surface Fermi arcs in Weyl and Dirac semimetals, Nat. Commun. 5, 5161 (2014).
- [41] M. Kargarian, M. Randeria, and Y.-M. Lu, Are the surface fermi arcs in Dirac semimetals topologically protected? PNAS 113, 8648 (2016).
- [42] P. Villar Arribi, J.-X. Zhu, T. Schumann, S. Stemmer, A. A. Burkov, and O. Heinonen, Topological surface states in strained Dirac semimetal thin films, Phys. Rev. B 102, 155141 (2020).